Biomed. Technik, 48 (2003), 122-129

U. Scheipers[1], H. Ermert[1], H.-J. Sommerfeld[2],
M. Garcia-Schürmann[2], K. Kühne[2], T. Senge[2], S. Philippou[3]

Ultrasonic Tissue Characterization for Prostate Diagnostics: Spectral Parameters vs. Texture Parameters

Sonohistologie für die Prostatadiagnostik: Vergleich von Spektral- und Texturparametern

[1]Lehrstuhl für Hochfrequenztechnik, Ruhr-Universität Bochum, Germany
[2]Urologische Universitätsklinik, Marienhospital Herne, Germany
[3]Institut für Pathologie, Augustakrankenanstalten Bochum, Germany

Key words: Prostate – ultrasound – urology – tissue characterization – sonohistology

An ultrasonic multifeature tissue characterizing system for the detection of prostate cancer is presented. The system is based on the processing of radio frequency (RF) ultrasonic echo data. Data from 100 patients was acquired in a clinical study. Parameters are extracted from the RF echo data and classified using two adaptive network-based fuzzy inference systems (FIS) working in parallel as a nonlinear classifier. Next to spectral parameters, conventional texture parameters are calculated using demodulated and log-compressed echo data. In the first approach, the classifier is trained on both, spectral and texture parameters. In the second approach, the classifier is only trained on texture parameters. Classification results of both approaches are compared and it is demonstrated, that only the use of spectral parameters yields satisfying classification results. Results of a minimum distance classifier (MDC) are presented for comparison with the fuzzy inference system. For the final fuzzy inference systems used in this approach, the area under the ROC curve is between 84 % and 86 % for the combined approach and between 70 % and 74 % for the approach based on texture parameters only.

Schlüsselwörter: Prostata, Ultraschall, Urologie, Gewebecharakterisierung, Sonohistologie

Ein Multiparameter-Sonohistologiesystem für die Erkennung von Prostatakarzinomen wird vorgestellt. Das System basiert auf der Verarbeitung von hochfrequenten (HF) Ultraschalldaten. In einer klinischen Studie wurden Daten von 100 Patienten erfaßt. Verschiedene gewebebeschreibende Parameter wurden aus den hochfrequenten Ultraschalldaten extrahiert und mit zwei parallel arbeitenden Fuzzy-Folgerungs-Systemen (FIS) klassifiziert. Neben Spektralparametern wurden konventionelle Texturparameter berechnet. Im ersten, kombinierten Ansatz werden sowohl Spektralals auch Texturparameter zum Anlernen des Klassifikators benutzt. Im zweiten Ansatz werden zum Vergleich lediglich Texturparameter für das Training benutzt. Die Klassifikationsergebnisse beider Ansätze werden miteinander verglichen, und es wird gezeigt, daß lediglich durch den Einsatz von Spektralparametern zufriedenstellende Ergebnisse erzielt werden können. Neben den Klassifikationsergebnissen der Fuzzy-Folgerungs-Systeme werden die Ergebnisse eines Minimum-Distanz-Klassifikators (MDC) vorgestellt, um einen Vergleich zwischen den Verfahren zu ermöglichen. Mit den Fuzzy-Folgerungs-Systemen wird für den kombinierten Ansatz eine Fläche unter der ROC-Kurve von 84 % bis 86 % erreicht, für den nur auf Texturparametern basierenden Ansatz wird lediglich eine Fläche von 70 % bis 74 % erreicht.

1 Introduction

The incidence of the prostate carcinoma is one of the highest in men in the western world [41]. Its position in cancer mortality statistics is also among the highest [7, 35, 36]. The prevalence found at autopsy suggests that the prostate carcinoma is the most common malignancy in human beings in the United States [43].

The different types of diagnostics that are used today (digital rectal examination, transrectal ultrasound imaging and prostate-specific antigen (PSA) value analysis) lack reliability and are therefore not sufficient. Even a combination of these three methods is not sufficiently reliable [43, 50, 1].

An automated classification system for prostate diagnostics based on multifeature tissue characterization is proposed. RF ultrasonic echo data is acquired during the standard transrectal ultrasound imaging examination. Several parameters are calculated and fed into two fuzzy inference systems (FIS) working in parallel. The outputs of the FIS are fed into a post processing procedure evaluating contextual information before being combined to form a malignancy map, in which areas of high cancer probability are marked in red. The malignancy map is presented to the physician during the examination to approve the early detection of prostate cancer.

During the last years, studies have been carried out dealing with the characterization of prostate tissue using ultrasound imaging. Some approaches are based on video or image data [3, 21, 17, 32, 33] and do not take into account the depth dependent diffraction and attenuation [21, 17, 32, 33]. Some authors tried to characterize prostate tissue by using only a single parameter, e.g. attenuation estimates [24, 25] or backscatter estimates or by combining different parameters using a lin-

ear approach or a nearest-neighbor technique [10, 11]. Some authors used nonlinear methods like neural networks [12, 13, 14, 2] and Kohonen maps [47] to combine the parameters and even compare different nonlinear methods with each other [34, 49]. An overview of ultrasonic tissue characterization in general can be found in [53, 6]. An overview of prostate diagnostics using ultrasound imaging is given in [50].

By using video data instead of RF data only a small set of analysis parameters can be calculated which do not contain enough information needed to classify the tissue with sufficient accuracy. Only the use of Radio-frequency (RF) data can provide the information used to calculate spectral parameters that characterize prostate tissue in an adequate way.

To prove this statement, two approaches are described in this work. The first approach is based on spectral and texture parameters, while the second approach, which is presented for comparison, only uses texture parameters.

As different parameters have a highly nonlinear interdependence, only a nonlinear model is able to combine the parameters and thus lead to reliable results [47, 32, 33, 26]. For this reason a neuro fuzzy inference system is used in this approach [58, 59, 22, 37, 16].

For the evaluation of parameters the compensation of depth dependent diffraction and attenuation effects has been found to be essential [40, 20, 30, 31, 49, 47, 39].

Some former works focus merely on the evaluation of one set of parameters, e. g. cooccurrence parameters [3] or spectral parameters [10, 11, 12, 2]. Other works try to combine the results of different sets of parameters [34, 49, 47, 48]. As the information of parameters of different sets is highly uncorrelated, the combination of parameters originating from different sets might lead to better classification results. From our point of view only a combination of different sets of parameters can provide the classification system with enough information to support a precise decision.

During the search for the best parameters it was found, that for a given depth of the ultrasound echo signal certain parameters perform better than others. This observation leads to the integration of some morphological descriptors, which serve as so-called morphological parameters describing the position of the regions of interest (ROI) within the prostate.

2 Methods

2.1 Data Acquisition and Preprocessing

RF ultrasonic echo data of the prostate is captured during the regular examination of the patient with standard ultrasound imaging equipment (Kretz Combison 330, transrectal probe VRW177AK). Patient compliance is high, as the new method does not extend the normal examination time when applying transrectal ultrasound imaging. The system is operator-independent, which means that no special knowledge or training is necessary for a successful application of the system. The RF data is captured from the ultrasound imaging system before being processed by the ultrasound imaging system's time gain control unit (TGC). The signal is fed into a custom-made hardware TGC with a known transfer function to compensate for depth dependent attenuation effects and to provide the following analog to digital converter (ADC) with a signal that uses the whole possible conversion range throughout the sampling time. After time variant amplification the data is directly transmitted to a PC and sampled at 33 MHz and 12 bits. During the next step, every A-line is compensated for the induced TGC amplification. Every data frame is subdivided into up to 1000 ROIs per prostate slice using sliding window technique, in order to attain spatially distributed tissue characterization images. Each ROI comprises an area of approximately 3.0 mm × 3.5 mm in diameter at a depth of 20 mm. The smallest lesion that can be detected by the system thus covers approximately 0.1 cm^2. The ROIs consist of 128 sample points in the transducers axial direction and 16 scan lines in the lateral direction. For attenuation measurements, adjacent ROIs are combined for each single estimation, as the ROI sizes mentioned above are too small to support a reliable attenuation estimation [49]. Their axial and lateral overlap is 75 % and 50 % respectively. Up to five datasets at different transducer positions are being recorded per patient.

The RF data is compensated for system and depth dependent effects using the system's point spread function over depth as an inverse filter within the system's effective bandwidth. Using this approach, it is possible to compensate partly for the system's effects due to focusing and for the electromechanical characteristics of the transducer [53].

2.2 Parameter Extraction

Several parameters are calculated for each ROI. The authors do not claim the extracted parameters to be totally independent of the ultrasound imaging equipment. The parameters used for classification are calculated from the frequency domain and from the time domain, partly before and partly after demodulation [56].

Overall, this approach is based on two parameter groups. The first group consists of spectral parameters, whereas the second group consists of texture parameters of first and second order.

Spectral parameters are calculated after converting the resultant power spectrum to dB [57]. Spectra of each scan line are averaged to form an estimate of the average power spectrum [29, 51]. The primary set of spectral parameters consists of four measures of backscatter calculated for the signal bandwidth. The parameters used in this approach are: slope, axis intercept, midband value and deviation of the linear regression spectrum fit [34, 44, 45, 46, 12]. The measures of backscatter are compensated for attenuation effects us-

Table 1. Classification results of spectral parameters for both groups, P1 and P2, and both approaches, FIS and MDC, in comparison. The area A_z under the ROC-curve is given next to the standard deviation σ of the estimates. Parameters that were used in the final systems are highlighted.

Spectral parameters	P1 FIS A_z	P1 FIS σ	P1 MDC A_z	P1 MDC σ	P2 FIS A_z	P2 FIS σ	P2 MDC A_z	P2 MDC σ
Backscatter parameters:								
Axis intercept	**0.590**	**0.014**	0.590	0.014	0.550	0.014	**0.549**	**0.013**
Slope	0.558	0.007	**0.552**	**0.008**	0.510	0.014	0.541	0.032
Midband value	**0.622**	**0.015**	**0.622**	**0.015**	**0.558**	**0.032**	0.547	0.028
Square deviation	0.512	0.001	0.509	0.001	0.500	0.006	0.512	0.005
Normalized sq. dev.	0.568	0.008	0.568	0.008	0.518	0.023	0.529	0.010
Attenuation estimates:								
Axis intercept	**0.612**	**0.005**	**0.609**	**0.004**	**0.555**	**0.014**	0.545	0.022
Slope	**0.548**	**0.018**	0.538	0.022	**0.554**	**0.006**	**0.556**	**0.011**
Midband value	0.583	0.003	**0.584**	**0.004**	0.557	0.042	0.537	0.016
Group classification:	0.773	0.005	0.640	0.017	0.646	0.027	0.583	0.051

ing an attenuation estimation model, which is based on the multi narrow band method [47, 5, 40, 52]. Three measures of this attenuation model are also included in the system. The attenuation parameters used in this approach are: slope, axis intercept and midband value. Classification results of the spectral parameters are given in Table 1.

Texture parameters consist of first and second order (i. e. cooccurrence) parameters. Texture parameters are calculated after demodulating the RF data using Hilbert transformation.

First order parameters consist of 11 different estimates of intensity: maximum, minimum, mean, standard deviation, contrast (variance), kurtosis, skewness, signal to noise ratio, ratio of squares, entropy and the full width at half maximum (*FWHM*) of the gray level histogram. Classification results of the first order texture parameters are given in Table 2.

Because of the sector geometry of the scan and possible diffraction effects, every parameter is evaluated in the axial direction only and averaged over all lines of the corresponding ROI.

Various parameters from common cooccurrence matrices (spatial gray-tone dependence matrices) as proposed by Haralick [18], Valckx and Thijssen [54] and Valckx et al. [55] are calculated in the spatial domain on demodulated data for different distances d, i. e. step sizes between pixels, up to $0.5 \cdot FWHM$ [44, 3]. Sizes of cooccurrence matrices, i. e. the number of gray levels incorporated, are varied.

For applications in image processing, orientation angles δ of 0°, 45°, 90° and 135° are typically calculated. When using a sector based ultrasound scanner, gray-tone spatial dependency matrices may only be calculated in axial direction because of the nonlinear geometry of the scan area. Even when using an ultrasound scanner with a linear geometry, the calculation of symmetric gray-tone spatial dependency matrices combining all directions may be doubtful because of focusing and diffraction reasons. Another problem is the dependence of some cooccurrence parameters on the linear attenuation of the system. Depth variant parameters used here are: correlation, inverse difference moment and variance. It is possible to compensate for the depth dependency by normalizing the data as proposed in [18] or by normalizing each ROI locally. All other cooccurrence parameters evaluated in this approach are independent of depth.

In contrast to first order texture parameters, second order texture parameters are based on spatial relations between pixel gray levels and can therefore describe spatial distributions of information in data. Second or-

Table 2. Classification results of first order texture parameters for both groups, P1 and P2, and both approaches, FIS and MDC, in comparison. The area A_z under the ROC-curve is given next to the standard deviation σ of the estimates. Parameters that were used in the final systems are highlighted.

First order texture parameters	P1 FIS A_z	P1 FIS σ	P1 MDC A_z	P1 MDC σ	P2 FIS A_z	P2 FIS σ	P2 MDC A_z	P2 MDC σ
Maximum	0.604	0.026	0.604	0.028	**0.560**	**0.038**	**0.559**	**0.026**
Minimum	**0.622**	**0.023**	0.619	0.024	0.539	0.034	0.546	0.011
Mean value	0.621	0.026	**0.621**	**0.026**	**0.555**	**0.036**	0.552	0.018
Ratio of squares	**0.590**	**0.012**	0.581	0.022	0.558	0.030	0.554	0.031
Signal to noise ratio	0.592	0.013	0.576	0.023	0.558	0.031	0.555	0.020
Standard deviation	**0.528**	**0.010**	0.524	0.011	0.527	0.007	**0.538**	**0.020**
Contrast/Variance	0.526	0.009	0.524	0.010	0.538	0.020	0.538	0.020
Full width at half max	**0.528**	**0.003**	0.522	0.005	0.525	0.002	0.523	0.002
Entropy	0.510	0.002	0.507	0.006	0.523	0.002	0.524	0.000
Kurtosis	0.519	0.006	**0.516**	**0.005**	0.529	0.010	0.533	0.011
Skewness	**0.538**	**0.004**	0.537	0.004	0.534	0.015	**0.532**	**0.015**
Group classification:	0.681	0.016	0.624	0.028	0.593	0.045	0.559	0.033

der texture parameters evaluated in this approach are: angular second moment, which is a measure of the local homogeneity of the data and represents the energy within the cooccurrence matrix, contrast, which is a measure of the amount of local variations present in the data and thus directly characterizes edges and specular structures, correlation, which is a measure of local linear dependencies and thus can be useful to characterize local periodic texture patterns, dimension, entropy, which is often used to characterize diffuse echoes and other highly disordered texture patterns, inverse difference moment, kappa, peak density and variance. Classification results of the second order texture parameters are given in Table 3.

Under certain circumstances, some parameters used in this approach may lead to unreliable results. For example, attenuation measurements fail, if data is taken from a region behind calcifications. Some cooccurence parameters that are independent of the mean intensity still yield satisfying results under these circumstances. Because calcifications are, in most cases, found in the lower section of the prostate, this observation led to the inclusion of morphological descriptors, thus allowing the fuzzy inference system to choose different parameter combinations for different positions. Morphological descriptors that are used in this approach are: distance of the ROI from the center of the ultrasound probe, normalized axial position of the ROI within the prostate and normalized lateral position of the ROI within the prostate. All parameters are normalized for the size of each individual prostate to yield a value between 0 and 1.

Initial results have shown that only a combination of spectral and texture parameters leads to adequate classification results [34, 47, 48].

2.3 Training procedure

Methods for estimating the accuracy of diagnostic tests require independence of the test results in the samples. For this reason, five-fold cross validation methods have been used for the selection and combination of parameters for the final tissue characterization system. Cross validation methods are known to yield a nearly unbiased prediction error, when accepting the disadvantage that the results can be highly variable [8]. In approaches where there are multiple cases from the same patient, estimation and inference of the accuracy of the diagnostic test must account for intracluster correlation. To account for intracluster correlation, the five-fold cross validation method has been used on five datasets, which were constructed considering a division of the amount of patients, not the amount of ROIs [38]. When using cross validation methods and not keeping in mind that possible intracluster correlations are apparent, the classification results will be far from reality as too positively weighted.

2.4 Selection of parameters

During the preselection procedure of parameters for the training process of the system, parameter vectors that are highly linearly dependent on each other are found and discarded using covariance matrix analysis. Parameter vectors that have a small influence on the classification procedure are found and discarded using single classification. During the preselection, the number of parameters is reduced to 13 for the first fuzzy inference system and to 10 for the second system, respectively, using a stepwise selection algorithm based on hypothesis testing. The parameter selection procedure starts by calculating the classification power of each single feature. In order to use a decision-based criterion [28] instead of an approximation-based criterion (e.g. mean square error) as used in other approaches, the classification power is expressed as the area A_z under the ROC-curve [27].

As the number of ROIs used in this work is high (about 170,000), using up to 13 parameters for the classification procedure is still a safe approach [15, 42, 4]. The „curse of dimensionality“ does not account for the settings of this approach, but it has to be considered, that, as several ROIs in this approach result from the same patients, the effective sample size is somewhere between the actual sample size and the number of patients.

Table 3. Classification results of second order (cooccurrence) texture parameters for both groups, P1 and P2, and both approaches, FIS and MDC, in comparison. The area A_z under the ROC-curve is given next to the standard deviation σ of the estimates. Parameters that were used in the final systems are highlighted.

Second order texture parameters	P1 FIS A_z	P1 FIS σ	P1 MDC A_z	P1 MDC σ	P2 FIS A_z	P2 FIS σ	P2 MDC A_z	P2 MDC σ
Angular second moment	0.596	0.014	0.596	0.015	0.519	0.021	0.532	0.023
Contrast	**0.640**	**0.020**	0.639	0.021	**0.507**	**0.018**	0.520	0.016
Correlation	0.537	0.022	0.535	0.022	**0.533**	**0.019**	**0.540**	**0.031**
Dimension	**0.642**	**0.020**	**0.641**	**0 021**	**0.510**	**0.018**	0.519	0.012
SNR	**0.598**	**0.015**	**0.595**	**0.015**	0.518	0.020	0.532	0.023
Inverse difference moment	0.609	0.017	0.609	0.018	0.505	0.014	0.519	0.013
Kappa	0.610	0.023	0.609	0.023	0.529	0.008	**0.530**	**0.009**
Peak Density	**0.576**	**0.016**	0.576	0.016	**0.510**	**0.018**	0.528	0.018
Variance	0.596	0.014	0.595	0 015	**0.521**	**0.023**	0.532	0.023
Group classification:	0.726	0.016	0.645	0.020	0.619	0.041	0.540	0.036

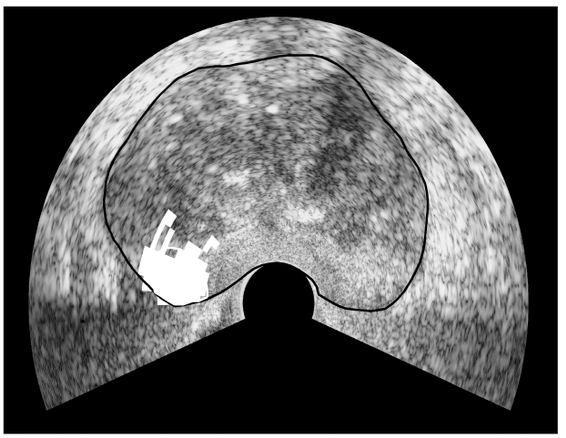

Figure 1. Overlay of B-mode image and malignancy map. Areas of a high cancer probability are marked white.

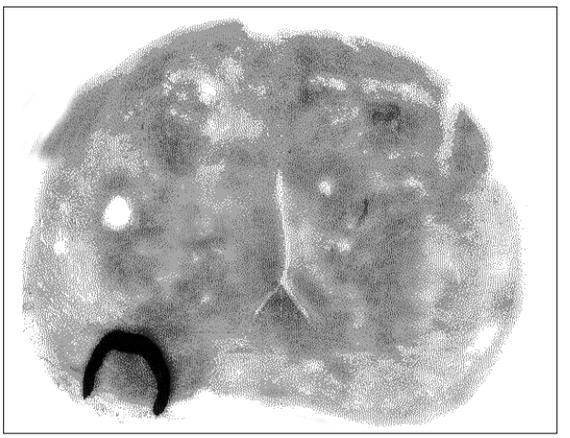

Figure 2. Histology, tumors have been stained, malignant and benign tissue areas have been marked by pathologist.

2.5 Fuzzy Inference Systems

Two FIS working in parallel classify and separate the ROIs into two classes (negative = benign, positive = malignant). Fundamentals of fuzzy logic and the idea behind this approach can be found in [58, 59, 37]. An overview of neuro-fuzzy systems is given by Jang in [23]. The mathematical background, especially the learning process of the FIS, is also described best by Jang in [23].

The fuzzy output maps of both fuzzy inference systems are transformed into binary maps applying a separation-threshold to separate into two classes. The separation-threshold can be chosen freely by the operator, as the implemented system is a quantitative system. Certainly, an amount of „information" is discarded during this step, but the output of the system becomes more readable by the physician. A following morphological analysis combines clusters in the binary output maps of the fuzzy inference systems to mark areas of similar tissue characteristics. The clustering procedure is implemented by two-dimensional filtering the binary output maps with symmetric 1/0-kernels of systematically determined size. During the training procedure, the optimal kernel sizes and filter-thresholds are determined. This is done by systematically varying kernel sizes and filter-thresholds and comparing the classification results to find the optimal combinations. The optimal kernel sizes and filter-thresholds are determined for the whole range of separation-thresholds, thus still allowing a free choice of separation-threshold during the evaluation procedure. Next to improving the classification rates by a small amount, this post-processing step makes the malignancy maps more readable by the physician.

The results of the two fuzzy inference systems are combined to build a so-called malignancy map, which consists of a conventional B-mode image, in which areas of high cancer probability are marked in red (white on printed matter). The malignancy map (Fig. 1) is presented to the physician during the examination on a PC screen and thus can support the existing methods of diagnostics. Malignancy maps can easily be printed or archived for biopsy planning.

3 Clinical study

During a clinical study, radio-frequency ultrasonic echo data of 100 patients undergoing clinical examinations was recorded. At the day of the examination the youngest patient was 48 years old, the oldest 79 years. Both, the mean and median age of the patients were 64 years. All patients of this study underwent radical prostatectomy. Prostate slices with histological diagnosis following radical prostatectomies act as the gold standard and „teacher data". Histological analysis is usually accepted as gold standard; nevertheless it is subject to error [19]. The concentration of the PSA in the patient's blood and the results of the digital rectal examination have also been recorded for cross validation reasons.

The PSA values of the patients were in the range of 1 ng/ml to 93 ng/ml, 17 patients had a PSA value greater than 20 ng/ml, which is a good indicator for the presence of prostate cancer. 21 patients had a PSA value between 20 ng/ml and 10 ng/ml, which still stands for a certain probability of prostate cancer. The greatest amount of patients, 49 in total, had a PSA value between 10 ng/ml and 4 ng/ml, an amount that makes concluding rather unreliable [43]. 9 patients had a PSA value below 4 ng/ml. No PSA values have been recorded for 4 patients.

Taking a look at the results of the digital rectal examination, about 44 patients had to be diagnosed T3, 41 patients were diagnosed T2 and 11 patients received a diagnosis of T1. One patient was diagnosed T4. No carcinoma could be diagnosed by digital palpation in 3 cases.

The RF datasets have been divided as described above resulting in a sum of 129,967 benign and 40,517 malignant ROIs.

After prostatectomy, a minimum of three prostate slices has been dissected for each patient while keeping the angle of the slices according to the angle of the ultrasound transducer during the data acquisition. Prostate tissues have been stained and marked on the prostate slices with hematoxylin and eosin. Malignant areas have been encircled by the pathologists (Fig. 2). The contours have been transferred to the PC by experi-

Table 4. Final classification results of FIS using leave-one-out cross validation for both groups, P1 and P2.

Parameter group	P1	P2
Spectral and texture parameters	0.861	0.840
Texture parameters	0.742	0.703

enced physicians thus making a more or less definite assignment of dataset ROIs to tissue classes possible (Fig. 3). For transferring the contours to the PC, the B-mode images of all recorded datasets of one patient are displayed on the PC screen. The physician chooses the datasets that fit the prostate slices best and transfers the contour to the PC, interactively encircling the prostate and cancerous areas with the mouse. Only datasets that exactly match the prostate slices are kept for further processing. This results in approximately two or three validated datasets per patient.

For classification reasons the tumors have been divided into two different classes. The first class P1 (positive) consists of all tumors that were visible in the classical B-mode image. All in all this class consists of 27,608 ROIs. Hypoechoic tumors have been included in this class as well as hyperechoic tumors. The second class P2 consists of all isoechoic tumors, which are tumors that are not visible in the conventional B-mode [9, 43]. That means these tumors appear in the B-mode image in the same manner as healthy tissue. Overall 12,909 ROIs belong to this class. Considering these amounts it can easily be concluded that about 1/3 of all tumors cannot be seen in conventional B-mode imaging. This result correlates with former studies on transrectal ultrasound imaging [50, 43]. Prior work has shown that partitioning of the entire amount of malignant ROIs into these two classes improves the classification results quite significantly [34].

The third class N (negative) consists of all other kinds of tissue. Next to ROIs of normal tissue also ROIs that consist of benign prostate hyperplasia belong to this class. Combining all kinds of tissues that do not belong to one of the two positive classes into one negative class is considered a good choice by means of designing a neuro fuzzy inference system. It has to be mentioned that also all other kinds of tissue, for example stones etc., belong to the class N. The manual transfer of prostate and tumor contours from prostate slices to the PC screen is a procedure that is very sensitive to errors. The physician has to work properly and precisely to keep transfer errors as low as possible during the training procedure. The transferring procedure can be conducted reasonably well for tumors that are more or less visible in the conventional B-mode image, but requires great skills from the physician in case of isoechoic tumors, thus allowing the physician only to use typical landmarks like the prostate border, stones and the seminal duct to navigate. During the preparation, prostate slices often are deformed making a proper correlation even more complicated. From the current point of view, an automatic transfer procedure, based on acquiring images of the histological prostate slices by using a scanner and digital image processing does not seem to be able to satisfy the demands that are required.

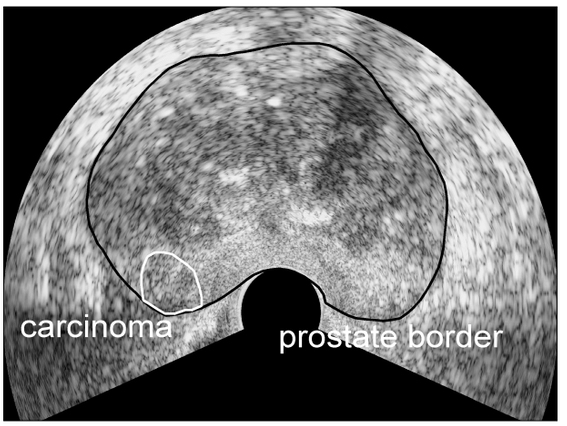

Figure 3. B-mode image with contours as transferred to the PC by the physicians.

4 Results

Two fuzzy inference systems were trained successively using the histological findings as „teacher data“. The first system was trained to distinguish the class P1, i.e. hypo- and hyperechoic tumors, from class N, i.e. „normal“ tissue. The second system was used to distinguish between the class P2, that is isoechoic tumors, from the class N. Each of both fuzzy inference systems yields a fuzzy value for each ROI of the ultrasound dataset. The fuzzy value is a measure of the probability of a ROI to be malignant or benign. As the classification procedure applied here represents a continuous system, sensitivities and specificities can be chosen freely under dependence on each other.

As can be seen in Table 4, the ROC curve area is $A_{Z1} = 0.86$ for the first system and $A_{Z2} = 0.84$ for the second system, respectively, when using both spectral and texture parameters for the systems. When only texture parameters are used for the training and validation, the ROC curve area is only $A_{Z1} = 0.74$ for the first system and $A_{Z2} = 0.70$ for the second system, respectively. The ROC curve area has been calculated by continuously varying the separation-threshold [38]. The capability of the system has been determined using the leave-one-out classification method, which means that the system has been trained on 99 patients to classify the remaining 100th patient [8]. After 100 single calculations, the results are averaged to form the final classification results.

An overview of different parameter performances is given in Tables 1, 2 and 3. Classification results are calculated for single parameter classification for both target groups P1 and P2, and for a combined classification involving all parameters of a group. This so-called group-classification points out that a single group of parameters cannot achieve the classification results of the final classification involving all groups of parameters.

Next to the classification results of the FIS, the results of a minimum distance classifier (MDC) are presented for comparison. The parameters that were used in the final system are highlighted in the tables.

5 Conclusion

It has been shown that our system for ultrasonic multifeature tissue characterization is able to detect prostate carcinoma with a high grade of accuracy. Thereby, the system can supplement the existing methods of prostate diagnostics to improve the early detection of prostate cancer and allow more reliable diagnostics. As can be seen in Table 4, the ROC curve area is $A_{Z1} = 0.86$ for the first system, which was trained to distinguish between hyperechoic, hypoechoic and normal tissue, and $A_{Z2} = 0.84$ for the second system, which was trained to distinguish between isoechoic tumors and normal tissue, respectively. Tumors that are not visible in the conventional B-mode image can be located. Biopsy planning can be improved, unnecessary biopsies can be avoided and performed biopsies can be guided more reliably.

Regarding the classification results as presented in Tables 1, 2, 3, and 4, it is apparent that only the use of spectral parameters can yield satisfying classification results. If only texture parameters are used for the classification, a maximum ROC are of only $A_{Z1} = 0.74$ for the first system and $A_{Z2} = 0.70$ for the second system, respectively, can be achieved using leave-one-out cross validation.

Considering these results, it is obvious that the use of RF data for ultrasonic tissue characterization is essential and cannot be substituted by using video data instead. From video data, only a small subset of parameters, i. e. texture parameters, can be calculated. It has to be mentioned, that all texture parameters used in our approach have been calculated after compensating for the system induced effects and after compensating for attenuation. When video-grabbed data is used instead, the classification results are expected to be even worse.

A comparison of the classification results of the FIS and the MDC classifier confirms the assumption that a nonlinear classifier is needed for the classification of the parameters used in this approach. For single parameter classification, the MDC still performs reasonably well. The advantage of the FIS is apparent, when different parameters are combined in a single system. A combination of different parameters from different parameter groups is only satisfactory when using a non-linear classifier like fuzzy inference systems or neural networks.

The problem with conventional B-mode ultrasound imaging for the detection of prostate cancer is the interobserver variability, i. e. the dependence of diagnostic results on the abilities of the physician [50]. A highly trained physician might be able to detect the majority of tumors, while a novice physician may tend to oversee tumors that are small or have isoechoic properties and can therefore not be seen in conventional B-mode imaging. An ultrasonic tissue characterization system can automate the process of finding suspicious regions and hence can help to reduce the wide gap in ultrasound imaging diagnosis results between expert and novice physicians. As the system evaluates characteristics of the ultrasonic echo signal that cannot be seen in the conventional B-mode image it may also be of great help to the expert. It has to be mentioned that a system for ultrasonic tissue characterization, as far as we can imagine, will not be able to totally replace the expert in finding a diagnosis, but it can significantly assist.

Acknowledgment

This work is an activity of the Kompetenzzentrum Medizintechnik Ruhr (KMR) and was supported by the Deutsche Forschungsgemeinschaft (DFG) grant ER 94/20-2.

References:

[1] Aarnink, R. G.; H. P. Beerlage, J. J. M. C. H. de la Rosette, F. M. J. Debruyne, H. Wijkstra: Transrectal Ultrasound of the Prostate: Innovations and Future Applications. The Journal of Urology 159 (1989), 1568–1579.

[2] Balaji, K. C.; W. R. Fair, E. J. Feleppa, C. R. Porter, H. Tsai, T. Iu, A. Kalisz, S. Urban, J. Gillespie: Role of Advanced 2 and 3-Dimensional Ultrasound For Detecting Prostate Cancer. The Journal of Urology 168 (2002), 2422–2425.

[3] Basset, O.; Z. Sun, J. L. Mestas, G. Gimenez: Texture Analysis of Ultrasonic Images of the Prostate by Means of Cooccurrence Matrices. Ultrasonic Imaging 15 (1993), 218–237.

[4] Chan, H. P.; B. Sahiner, R. F. Wagner, N. Petrick, J. Mossoba: Effects of Sample Size on Classifier Design: Quadratic and Neural Network Classifiers. Proceedings of SPIE Medical Imaging 3034 (1997), 1102–1113.

[5] Cloostermans, M. J. T. M.; J. M. Thijssen: A Beam Corrected Estimation of the Frequency Dependent Attenuation of Biological Tissues from Backscattered Ultrasound. Ultrasonic Imaging 5 (1983) 2, 136–147.

[6] Delorme, S.; I. Zuna: Ad multos annos. Ultraschall in Med 21 (2000), 230–232.

[7] Denmeade, S. R.; J. T. Isaacs: A History of Prostate Cancer Treatment. Nature Reviews: Cancer 2 (2002), 389–396.

[8] Efron, B.; R. Tibshirani: Improvements on Cross-Validation: The .632+ Bootstrap Method. Journal of the American Statistical Associations 92 (1997) 438.

[9] Ellis, W. J.; M. K. Brawer: The Significance of Isoechoic Prostatic Carcinoma. The Journal of Urology 152 (1994), 2304–2307.

[10] Feleppa, E. J.; A. Kalisz, J. B. Sokil-Melgar, F. L. Lizzi, Tian Liu, A. L. Rosado, M. C. Shao, W. R. Fair, Yu Wang, M. S. Cookson, V. E. Reuter, W. D. W. Heston: Typing of Prostate Tissue by Ultrasonic Spectrum Analysis. IEEE Transactions on Ultrasonics, Ferroelectrics, and Frequency Control 43 (1996) 4, 609–619.

[11] Feleppa, E. J.; Tian Liu, A. Kalisz, M. C. Shao, N. Fleshner, V. Reuter, W. R. Fair: Ultrasonic Spectral-Parameter Imaging of the Prostate. International Journal of Imaging Systems & Technology 8 (1997) 1, 11–25.

[12] Feleppa, E. J.; W. R. Fair, Tian Liu, A. Kalisz, W. Gnadt, F. L. Lizzi, K. C. Balaji, C. C. Porter, H. Tsai: Two-dimensional and Three-dimensional Tissue-Type Imaging of the Prostate Based on Ultrasonic Spectrum Analysis and Neural-Network Classification. Medical Imaging: Ultrasonic Imaging and Signal Processing, SPIE, Washington (2000).

[13] Feleppa, E. J.; J. A. Ketterling, A. Kalisz, S. Urban, C. R. Porter, J W. Gillespie, P. B. Schiff, R. D. Ennis, C. S. Wuu, W. R. Fair: Advanced Ultrasonic Tissue-Typing and Imaging based on Radio-Frequency Spectrum Analysis and Neural-Network Classification for Guidance of Therapy and Biopsy Procedures. Proceedings of CARS (2001), 333–337.

[14] Feleppa, E. J.; R. D. Ennis, P. B. Schiff, C. S. Wuu, A. Kalisz, J. A. Ketterling, S. Urban, T. Liu, W. R. Fair, C. R. Porter, J. R. Gillespie: Spectrum-Analysis and Neural-Networks for Imaging to Detect and Treat Prostate Cancer. Ultrasonic Imaging 23 (2001),135–146.

[15] Foley, D. H.: Considerations of Sample and Feature Size. IEEE Transactions on Information Theory IT-18 (1972) 5, 618–626.

[16] Furuhashi, T: Fusion of Fuzzy/Neuro/Evolutionary Computing for Knowledge Acquisition. Proceedings of the IEEE 89 (2001) 9, 1266–1274.

[17] Giesen, R. J. B.; A. L. Huynen, R. G. Aarnink, J. J. M. C. H. de la

Rosette, C. v. d. Kaa, G. O. N. Oosterhof, F. M. J. Debruyne, H. Wijkstra: Computer Analysis of Transrectal Ultrasound Images of the Prostate for the Detection of Carcinoma: A Prospective Study in Radical Prostatectomy Specimens. The Journal of Urology 154 (1995), 1397–1400.

[18] Haralick, R. M.; K. Shanmugam, I. Dinstein: Textural Features for Image Classification. IEEE Transactions Syst. Man. Cybern SMC-3 (6) (1973), 768–780.

[19] Hoppin, J. W.; M. A. Kupinski, G. A. Kastis, E. Clarkson, H. H. Barrett: Objective Comparison of Quantitative Imaging Modalities Without the Use of a Gold Standard. IEEE Transactions on Medical Imaging 21 (2002) 5, 441–449.

[20] Huisman, H. J.; J. M. Thijssen: Precision and Accuracy of Acoustospectrographic Parameters. Ultrasound in Medicine and Biology 22 (1996) 7, 855–871.

[21] Huynen, A. L.; R. J. B. Giesen, J. J. M. C. H. De La Rosette, R. G. Aarnink, F. M. J. Debruyne, H. Wijkstra: Analysis of Ultrasonographic Prostate Images for the Detection of Prostatic Carcinoma: the Automated Urologic Diagnostic Expert System. Ultrasound in Medicine & Biology, UK 20 (1994) 1, 1-10.

[22] Jang, J.-S. R.: ANFIS: Adaptive Network-based Fuzzy Inference Systems. IEEE Transactions on Systems, Man, and Cybernetics 23 (1993) 3, 665-685.

[23] Jang, J.-S. R.; C.-T. Sun: Neuro Fuzzy Modeling and Control. Proceedings of the IEEE, 83 (1995) 3, 378-406.

[24] Jenderka, K. V.; T. Gärtner, M. Zacharias, H. Heynemann, U. Cobet: System Independent Tissue Typing of Human Testis and Prostate. Proceedings of the IEEE Ultrasonics Symposium 2 (1999), 1377-1380.

[25] Jenderka, K. V.; T. Gärtner, U. Cobet, M. Zacharias, H. Heynemann: Tissue Characterization by Imaging the Local Frequency Dependent Relative Backscatter Coefficient. Ultrasonic Imaging and Signal Processing, Proceedings of SPIE 3982 (2000), 270-277.

[26] Kadah, Y. M.; A. A. Farag, J. M. Zurada, A. M. Badawi, A. B. M. Youssef: Classification Algorithms for Quantitative Tissue Characterization of Diffuse Liver Disease from Ultrasound Images. IEEE Transactions on Medical Imaging 15 (1996) 4, 466-478.

[27] Kroschel, K.: Statistische Nachrichtentechnik. Berlin, Springer-Verlag 1996.

[28] Kung, S. Y.; J. S. Taur: Decision-Based Neural Networks with Signal/Image Classification Applications. IEEE Transactions on Neural Networks 6 (1995) 1, 170-181.

[29] Lang, M; H. Ermert, L. Heuser: In Vivo Study of On-line Liver Tissue Classification Based on Envelope Power Spectrum Analysis. Ultrasonic Imaging 16 (1994), 77-86.

[30] Lizzi, F. L.; M. Astor, E. J. Feleppa, M. Shao, A. Kalisz: Statistical Framework for Ultrasonic Spectral Parameter Imaging. Ultrasound in Medicine and Biology 23 (1997) 9, 1371-1382.

[31] Lizzi, F. L.; E. J. Feleppa, M. Astor, A. Kalisz: Statistics of Ultrasonic Spectral Parameters and Liver Examinations. IEEE Transactions on Ultrasonics, Ferroelectrics, and Frequency Control 44 (1997) 4, 935-942.

[32] Loch, T.; I. Leuschner, C. Genberg, K. Weichert-Jacobsen, F. Küppers, E. Yfantis, M. Evans, V. Tsarev, M. Stöckle: Artificial Neural Network Analysis (ANNA) of Prostatic Transrectal Ultrasound. The Prostate 39 (1999), 198-204.

[33] Loch, T.; I. Leuschner, C. Genberg, K. Weichert-Jacobsen, F. Küppers, M. Retz, J. Lehmann, E. Yfantis, M. Evans, V. Tsarev, M. Stöckle: Weiterentwicklung des transrektalen Ultraschalls. Der Urologe [A] 4 (2000), 341-347.

[34] Lorenz, A.; M. Blüm, H. Ermert, T. Senge: Comparison of Different Neuro-Fuzzy Classifi-cation Systems for the Detection of Prostate Cancer in Ultrasonic Images. Proceedings of the IEEE Ultrasonics Symposium (1997), 1201-1204.

[35] Lubold, H.-J.; J. E. Altwein, K.-H. Bichler, D. Czaja, J. Hüsing, P. Fornara, K.H. Jöckel, G. Lübben, K.Schalkhäuser, L. Weißbach, M. Wirth, H. Rübben: Screening for Early Prostate Cancer in Germany. Preliminary results of a Prospective Multicenter Trial. Der Urologe [A] 38 (1999), 114-123.

[36] Luboldt, H.-J.; H. Rübben: PSA-Based Early Detection of Prostate Cancer. Der Urologe [A] 39 (2000), 20-26.

[37] Mendel, J. M.: Fuzzy Logic Systems for Engineering: A Tutorial. Proceedings of the IEEE 83 (1995) 9, 345-377.

[38] Obuchowski, N. A.: Nonparametric Analysis of Clustered ROC Curve Data. Biometrics 53 (1997), 567-578.

[39] Oelze, M. L.; W. D. O'Brien, Jr.: Frequency-Dependent Attenuation-Compensation Functions for Ultrasonic Signals Backscattered from Random Media. J. Acoust. Soc. Am. 11 (2002) 5, 2308-1319.

[40] Oosterveld B. J.; J. M. Thijssen, P. C. Hartman, R. L. Romijn, G. J. E. Rosenbusch: Ultra-sound Attenuation and Texture Analysis of Diffuse Liver Disease: Methods and Prelimi-nary Results. Physics in Medicine & Biology 36 (1991) 8, 1039-1064.

[41] Peto, J.: Cancer Epidemiology in the Last Century and the Next Decade. Nature 411 (2001), 390-395.

[42] Ripley, B. D.: Pattern Recognition and Neural Networks. Cambridge University Press, UK (1996).

[43] Scardino, P. T.: Early Detection of Prostate Cancer. Urologic Clinics of North America 16 (1998) 4, 635-656.

[44] Scheipers, U.; A. Lorenz, A. Pesavento, H. Ermert, H. J. Sommerfeld, M. Garcia-Schürmann, T. Senge, S. Philippou: Ultraschall-Gewebecharakterisierung für die Prostatadiagnostik. Biomedizinische Technik 46 (2001) 1, 72-73.

[45] Scheipers, U.; H. Ermert, A. Lorenz, H. J. Sommerfeld, M. Garcia-Schürmann, T. Senge, S. Philippou: Ultraschall-Gewebecharakterisierung für die Früherkennung von Prostatatumoren. Ultraschall in Med 22 (2001) 1, 43.

[46] Scheipers, U.; H. Ermert, A. Lorenz, A. Pesavento, H. J. Sommerfeld, M. Garcia-Schürmann, K. Kühne, T. Senge, S. Philippou: Ultrasonic Multifeature Tissue Characterization for Prostate Diagnostics. Proceedings in Acoustics, DAGA (2002),689-690.

[47] Schmitz, G.; H. Ermert, T. Senge: Tissue Charac-teri-zation of the Prostate Using Kohonen-Maps. Proc. IEEE Ultrasonics Symposium (1994), 1487-1490.

[48] Schmitz, G.; H. Ermert, T. Senge: Color-Coded Tissue Characteri-zation Images of the Prostate. in P. Tortoli and L. Masotti. Acoustical Imaging 22 (1996), 459-464.

[49] Schmitz, G.; H. Ermert, T. Senge: Tissue Characterization and Imaging of the Prostate using Radio Frequency Ultrasonic Signals. IEEE Trans. Ultrasonics, Ferroelectrics, and Frequency Control 46 (1999), 126-138.

[50] Sedelaar, P. M.; P. L. M. Vijverberg, T. M. De Reijke, J. J. M. C. H. de la Rosette, P. J. M. Kil, J. G. Breackman, A. J. M. Hendrikx: Transrectal Ultrasound in the Diagnosis of Prostate Cancer: State of the Art and Perspectives. European Urology 40 (2001), 275-284.

[51] Thijssen, J. M.: Ultrasonic Tissue Characterization and Echographic Imaging. Phys. Med. Biol 34 (1989) 11, 1667-1674.

[52] Thijssen, J. M.; B. J. Oosterveld, P. C. Hartman, G. J. Rosenbusch :Correlations between Acoustic and Texture Parameters from RF and B-mode Liver Echograms. Ultrasound in Medicine and Biology 19 (1993) 1, 13-20.

[53] Thijssen, J. M.: Spectroscopy and Image Texture Analysis. Ultrasound in Medicine and Biology 26 (2000) 1, 41-44.

[54] Valckx, F. M. J.; J. M. Thijssen: Characterization of Echographic Image Texture by Cooccurrence Matrix Parameters. Ultrasound in Medicine and Biology 23 (1997) 4, 559-571.

[55] Valckx, F. M. J.; J. M. Thijssen, A. J. van Geemen, J. J. Rotteveel, R. Mullaart: Calibrated Parametric Medical Ultrasound Imaging. Ultrasonic Imaging 22 (2000), 57-72.

[56] Wagner, R. F.; S. W. Smith, J. M. Sandrik, H. Lopez: Statistics of Speckle in Ultrasound B-Scans. IEEE Transactions on Sonics and Ultrasonics 30 (1983) 3, 156-163.

[57] Wear, K. A.: A Gaussian Framework for Modeling Effects of Frequency-Dependent Attenuation, Frequency-Dependent Scattering, and Gating", IEEE Trans. Ultrasonics, Ferroelectrics, and Frequency Control, Vol. 49, No. 11, pp. 1572-1582, November 2002.

[58] Zadeh, L.A.: Outline of a new approach to the analysis of complex systems and decision processes. IEEE Transactions on Systems, Man, and Cybernetics 3 (1973) 1, 28-44.

[59] Zadeh, L.A.: Knowledge representation in fuzzy logic. IEEE Transactions on Knowledge and Data Engineering 1 (1989), 89-100.

1129

Address of Correspondence:
Dipl.-Ing. Ulrich Scheipers
Institute of High Frequency Engineering
Ruhr-University Bochum, IC 6/133
D-44780 Bochum
Germany
ulrich.scheipers@rub.de